Elastic and spinodal instabilities in strained periodic states: A phase-field-crystal study

K. R. Elder,[1] Brendan Aaron,[1] Vidar Skogvoll,[2] and Luiza Angheluta[3]
[1]*Department of Physics, Oakland University, Rochester, Michigan 48309, USA*
[2]*Department of Physics, University of Oslo, 0371 Oslo, Norway*
[3]*Njord Centre, Department of Physics, University of Oslo, 0371 Oslo, Norway*

(Received 12 June 2026; accepted 4 August 2026; published 20 August 2026)

The stability of periodic states under applied strain is investigated using the one-dimensional phase-field-crystal (PFC) model. We perform a linear stability analysis of periodic states within the one-mode approximation and identify a marginal zero-wave-number mode, corresponding to the global translational symmetry, which controls the onset of instability at long wavelengths. Two distinct instability mechanisms are found. At low mean densities, phase fluctuations in the complex amplitude dominate, leading to a phase (elastic) instability of the periodic state. At higher densities, amplitude softening and density fluctuations drives a spinodal-like melting and the onset of liquid-solid coexistence. The crossover between these two regimes occurs at a sharp threshold coinciding with the onset of coexistence, and is confirmed by direct numerical simulations of the full PFC dynamics. Our results clarify how mean density and strain control the loss of periodic order through competing elastic (phase) and amplitude-driven instabilities.

DOI: 10.1103/19bb-bqcd

I. INTRODUCTION

How crystalline materials lose stability and melt is important for understanding material properties. In equilibrium, and in the absence of applied strain, melting is controlled by thermal fluctuations. In this case, the crystalline state becomes unstable through the nucleation and growth of the liquid phase, or in low-dimensional systems, through defect-mediated mechanisms such as the Kosterlitz-Thouless transition [1,2], where the unbinding of thermally activated topological defects destroys long-range crystal order. In contrast, when a crystalline system is driven out of equilibrium by applied strain or stress, the loss of stability is no longer governed solely by thermal melting, but instead by mechanical instabilities. Metastable periodic states can lose stability through defect-mediated processes where localized phase slips, dislocations pairs or loops (depending on dimension) form in response to applied strains [3–10]. At sufficiently large driving rates, such as in high strain-rate experiments (e.g., spallation) and simulations, it has been proposed that melting may instead proceed via a spinodal-like mechanism [11,12] or virtual melting [13–17]. In this regime, the periodic state becomes linearly unstable to melting through the growth of unstable modes, rather than through the nucleation of isolated defects. This behavior is intrinsically nonequilibrium in nature and reflects the dynamical destabilization of the solid under rapid loading. These observations point to a broader unresolved challenge to develop a unified understanding of the governing instability transitions between phase-dominated (defect-mediated) and amplitude-density (spinodal-like) modes in strained crystalline states. Determining the conditions under which each mechanism dominates, and how this crossover is encoded in the structure of the system's linear modes, remains an open challenge. A clearer understanding of this crossover regime could help predict critical failure strains in crystalline solids, and guide the processing conditions of new materials where thermal and mechanical effects are present. In this work, we address this within the one-dimensional phase-field-crystal (PFC) model [18–20]. The PFC framework captures atomic-scale periodicity evolving on diffusive timescales, and naturally incorporates elasticity, phase transitions, and defect dynamics within a unified free-energy-based description [10,21,22]. The model is formulated in terms of a free-energy functional $\mathcal{F}[\psi]$, where ψ is a coarse-grained atomic number density difference field that is periodic in the crystalline phase and homogeneous in the liquid phase. To analyze the stability of strained periodic states, we employ a one-mode amplitude representation of the density field, i.e., $\psi = \psi_o + Ae^{iqx} + A^*e^{-iqx}$, where A is a complex amplitude and ψ_o is a slowly varying mean density. This representation separates amplitude magnitude and phase, enabling a direct characterization of the modes responsible for instabilities. Our analysis focuses on the linear stability of strained periodic states showing that the nature of the instability is governed by a soft (marginal) mode associated with the continuous symmetries of the PFC free energy. At zero wave number ($Q = 0$), this mode corresponds to a global phase shift of the periodic lattice. At finite and small wave number (long wavelength $0 < Q \ll 1$), this degeneracy is lifted, and instability develops as a spatially modulated extension of this symmetry mode. For small mean densities, fluctuations in the amplitude magnitude $|A|$ and density ψ_o are energetically costly, and the soft mode corresponds to the phase of the amplitude. As a result, the instability is governed by spatial modulations of the phase, corresponding to variations of the elastic displacement and hence to an *elastic instability*. In this regime, the lattice loses stability through localized phase instabilities, consistent with defect-mediated melting. Specifically in the limit $\bar{\psi}_o = 0$, three distinct modes can be identified; *diffusive*, *amplitude,* and *phase*. Essentially,

the diffusive modes at wave number Q describe mass diffusion and relax exponentially $\sim e^{-DQ^2t}$, where D is the diffusion constant. The amplitude mode is always stable, while the phase mode gives rise to a strain-induced instability, mediated by the nucleation of phase slips (loss or gain of a wavelength) which first occurs near $Q = 0$. For larger mean densities, as the system approaches the coexistence region between periodic and homogeneous phases, the character of the soft mode changes. The energetic cost of amplitude magnitude and density fluctuations $(\delta|A|, \delta\psi_o)$ is reduced, leading to a softening of the amplitude magnitude and its coupling to the mean density. The instability is no longer dominated by phase fluctuations, but instead shifts toward coupled amplitude/density modes. This behavior is characteristic of *spinodal-like instabilities*, where melting proceeds via a collective loss of crystalline order. By tracking the largest eigenvalue of the linearized system, we determine the critical quench depth at which the periodic state becomes unstable. This analysis reveals a density-dependent crossover between phase-dominated (elastic) and amplitude-density (spinodal) instabilities, and quantifies how strain ϵ, mean density $\bar{\psi}_0$, and quench depth jointly control the onset of melting. The remainder of the paper is organized as follows. In Sec. II, we introduce the PFC model and its amplitude formulation. Section III presents the linear stability analysis for homogeneous and periodic states, emphasizing the role of the marginal mode and its finite, but small Q extension. Section IV discusses the resulting stability boundaries and compares analytic predictions with numerical simulations. Finally, Sec. V summarizes the main results and their implications for defect nucleation and melting mechanisms.

II. PHASE-FIELD-CRYSTAL MODEL

For simplicity, we consider the one-dimensional phase-field-crystal (PFC) model [18–20], where the dynamics of the field related to the number density difference, ψ, is governed by the conserved Swift-Hohenberg or PFC equation, which in dimensionless form is given by

$$\frac{\partial\psi}{\partial t} = \partial_{xx}\frac{\delta F}{\delta\psi} = \partial_{xx}\left[\Delta B\psi + \mathcal{L}_0^2\psi + \psi^3\right], \tag{1}$$

where the free energy functional is

$$\mathcal{F}[\psi] = \int dx\left[\frac{\Delta B}{2}\psi^2 + \frac{\psi}{2}\mathcal{L}_0^2\psi + \frac{\psi^4}{4}\right], \tag{2}$$

with $\mathcal{L}_0 = 1 + \partial_{xx}$. The parameter ΔB acts as an effective temperature controlling the transition from homogeneous ($\psi =$ constant) to periodic states. Details on dimensional analysis are included in Appendix A and a discussion of the connection of model parameters to microscopic and mesoscopic quantities can be found in Ref. [8].

a. Zero-strain equilibria. Periodic equilibrium solutions of Eq. (1) can be approximated using a one-mode ansatz

$$\psi(x,t) = \bar{\psi}_o + Ae^{iqx} + A^*e^{-iqx}, \tag{3}$$

where $\bar{\psi}_o$ is the mean density, A is a spatially uniform complex amplitude and the equilibrium state is defined by $q = 1$. This approximation is accurate for small $|\Delta B|$ and $|\bar{\psi}_o|$, where higher harmonics are negligible. Minimizing the free energy F with respect to A and q gives

$$A_0 = \sqrt{-\frac{\Delta B + 3\bar{\psi}_o^2}{3}}, \tag{4}$$

which exists only for $\Delta B + 3\bar{\psi}_o^2 < 0$. This condition defines the existence of periodic states.

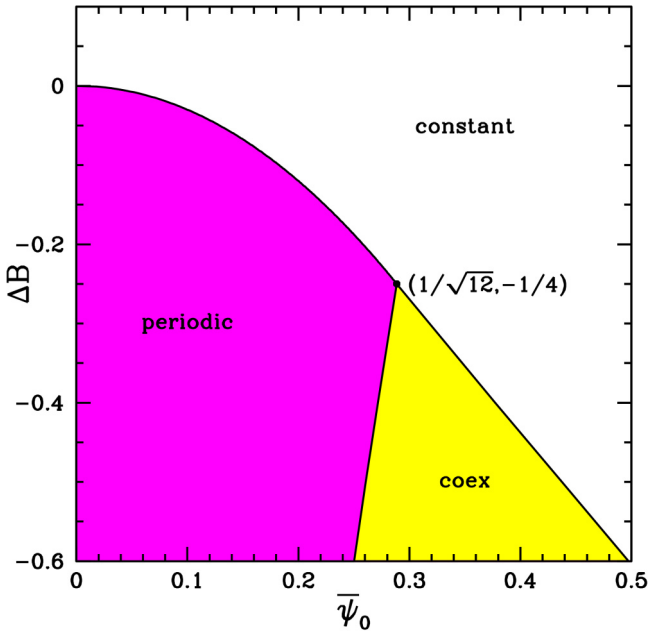

FIG. 1. Phase diagram for one-dimensional PFC model. As depicted in the diagram the equilibrium state is either a constant state (white region), periodic state (purple region), or a coexistence of the constant and periodic states (yellow region).

The phase diagram in Fig. 1, obtained by a Maxwell's equal-area construction [19], contains three distinct regions: (i) periodic states, (ii) homogeneous state, and (iii) a coexistence phase between periodic and homogeneous states (yellow in phase diagram). The phase boundary starting at $(\Delta B, \bar{\psi}_o) = (0, 0)$ and terminating at the point $(\Delta B, \bar{\psi}_o) = (1/\sqrt{12}, -1/4)$ is a line of second-order phase transitions, described by $\Delta B = -3\bar{\psi}_o^2$. Below this point a coexistence region (between periodic and constant states) exists, where phase boundaries correspond to first-order phase transitions.

b. Nonzero-strain equilibria. When a periodic state is strained its energy is raised, which in turn alters its stability. In PFC models mechanical strain is introduced through a shift in the wave number, $q = 1/(1+\varepsilon)$, where ε is the applied strain. To analyze weakly nonuniform states, we employ the one-mode amplitude formulation (APFC) with slowly varying mean density $\psi_o(x,t)$ and amplitude $A(x,t)$:

$$\psi(x,t) = \psi_o(x,t) + A(x,t)e^{iqx} + A^*(x,t)e^{-iqx}.$$

Substituting into Eq. (1) and averaging over one wavelength gives the evolution equations

$$\frac{\partial\psi_o}{\partial t} = \partial_{xx}\left[(\Delta B + 6|A|^2 + (1+\partial_{xx})^2)\psi_o + \psi_o^3\right], \tag{5}$$

$$\frac{\partial A}{\partial t} = \mathcal{L}\left[\Delta B + 3\psi_o^2 + 3|A|^2 + (1+\mathcal{L})^2\right]A, \tag{6}$$

where $\mathcal{L} \equiv \partial_{xx} + 2iq\partial_x - q^2$. Details of this derivation can be found in, e.g., Ref. [8]. Written in this form, both unstrained and uniformly strained states ($q \neq 1$), can be described by A being a real constant, which is advantageous for the stability analysis presented in the next section.

A uniform steady-state solution of Eqs. (5) and (6) corresponding to a strained periodic state is given by

$$A_s = \sqrt{\frac{-\omega_q}{3}}, \quad \psi_o = \bar{\psi}_o, \tag{7}$$

with $\omega_q = \Delta B + 3\bar{\psi}_o^2 + (1-q^2)^2$. Real solutions require $\omega_q < 0$, yielding the spinodal condition

$$\Delta B < -3\bar{\psi}_0^2 - (1-q^2)^2. \tag{8}$$

The first term in the above equation ($-3\bar{\psi}_o^2$) accounts for the lowering of the melting temperature with an increase in density and exactly matches the coexistence line shown in Fig. 1 from $(\bar{\psi}_o, \Delta B) = (0, 0)$ to $(1/\sqrt{12}, -1/4)$. In addition to this thermodynamic contribution, strain also shifts the stability boundary by $(1-q^2)^2 \approx 4\varepsilon^2$ for small ε, effectively lowering the melting temperature. Accordingly, ω_q can be interpreted as an effective temperature that includes both thermodynamic (ΔB, $\bar{\psi}_0$) and mechanical strain (q) contributions.

An effective diagram can be constructed using Maxwell's equal area construction, by fixing the solid to be strained. This effective diagram does not represent a true equilibrium phase diagram, since a strained state immersed in a liquid background would relax to its equilbrium lattice constant and eventually the system would obey the phase boundaries shown in Fig. 1. Nevertheless, it illustrates the consequences of strain on the thermodynamic behavior of the system. As shown in this figure, under an applied strain, the coexistence region extends toward $\bar{\psi}_o = 0$, and the second-order transition line is eliminated. A representative coexistence curve for for $\varepsilon = -0.0909$ and -0.0476 is shown in Fig. 2, illustrating the combined influence of thermodynamic and mechanical effects on stability.

III. STABILITY OF PERIODIC STATE: EIGENVALUE PROBLEM

One of the advantages of the APFC formulation is that the steady-state solutions are uniform, which simplifies the linear stability analysis by avoiding a Floquet treatment. To determine the stability of the steady-state strained periodic state, we introduce small perturbations,

$$\psi_o = \bar{\psi}_o + \delta\psi_o,\ A = A_s + \delta A,\ A^* = A_s + \delta A^*, \tag{9}$$

and linearize the equations of motion, Eqs. (5) and (6), with respect to $\delta\psi_o$, δA, and δA^*. By a Fourier transformation, each mode with wave number Q evolves independently as

$$\frac{d}{dt}\begin{pmatrix}\delta\hat{\psi}_o\\ \delta\hat{A}\\ \delta\hat{A}^*\end{pmatrix} = \mathbf{M}_Q \begin{pmatrix}\delta\hat{\psi}_o\\ \delta\hat{A}\\ \delta\hat{A}^*\end{pmatrix}, \tag{10}$$

where the evolution matrix $\mathbf{M}_Q$ is (derivation in the Appendix)

$$\mathbf{M}_Q = \begin{bmatrix} -Q^2(\omega_Q - 2\omega_q) & -Q^2\beta & -Q^2\beta \\ \hat{\mathcal{L}}_Q\beta & \hat{\mathcal{L}}_Q(\omega_{q+Q} - 2\omega_q) & -\hat{\mathcal{L}}_Q\omega_q \\ \hat{\mathcal{L}}_{-Q}\beta & -\hat{\mathcal{L}}_{-Q}\omega_q & \hat{\mathcal{L}}_{-Q}(\omega_{q-Q} - 2\omega_q) \end{bmatrix}, \tag{11}$$

where

$$\begin{aligned}\omega_{q\pm Q} &= \omega_q + (1-(q\pm Q)^2)^2 - (1-q^2)^2,\\ \omega_Q &= \omega_q + (1-Q^2)^2 - (1-q^2)^2\end{aligned} \tag{12}$$

using the notation $\beta \equiv 6\bar{\psi}_o A_s$ and $\hat{\mathcal{L}}_{\pm Q} = -(Q \pm q)^2$.

Normal modes $\sim e^{\lambda t}$ are solutions to the eigenvalue problem $\mathbf{M}_Q\vec{v} = \lambda\vec{v}$, where the three eigenvalues λ_i are determined by solving the characteristic equation $\det|\mathbf{M}_Q - \lambda\mathbf{I}| = 0$. Stability is determined by the spectrum $\lambda_i(Q)$, i.e., the periodic state is linearly unstable if $\mathrm{Re}(\lambda_i) > 0$ for any $i = 1, 2$, or 3 and Q.

A. Long-wavelength limit and mode classification

The eigenvalues can be Taylor expanded in small Q (i.e., long-wavelengths limit) and given by (see Appendix. C)

$$\lambda_i = -a_i - b_i Q^2 + \mathcal{O}(Q^4). \tag{13}$$

One eigenvalue satisfies $a_1 > 0$ (specifically $a_1 = -2q^2\omega_q > 0$) and remains strictly negative. The remaining two satisfy $a_{2,3} = 0$, yielding

$$\lambda_1(0) < 0, \quad \lambda_2(0) = \lambda_3(0) = 0. \tag{14}$$

Thus, the eigenvalue spectrum at $Q = 0$ consists of one stable mode and a two-dimensional neutral subspace. These neutral modes reflect underlying symmetries of the PFC model, i.e., the free energy is invariant to uniform shifts in ψ_o and global phase rotations of A. The stability of the periodic state is therefore governed by how this degeneracy is lifted at finite Q.

At small but finite Q, one mode remains stable ($b_2 > 0$), while the second becomes unstable when b_3 changes sign. Near the transition,

$$\lambda_3(Q) \simeq -[b_3(q) + c_3(q)Q^2]Q^2, \tag{15}$$

with $c_3(q) > 0$. Instability occurs when $b_3(q) < 0$, leading to growth in a band of long wavelengths as shown in Fig. 3.

Figure 3 shows representative eigenvalue spectra for the crystal state $(\Delta B, \bar{\psi}_o) = (-0.1374, 0.2)$ as a function of Q, for three values of the crystal wave number q near the instability threshold: below ($q = 1.029$), at ($q \approx 1.030$), and above ($q = 1.031$) the transition.

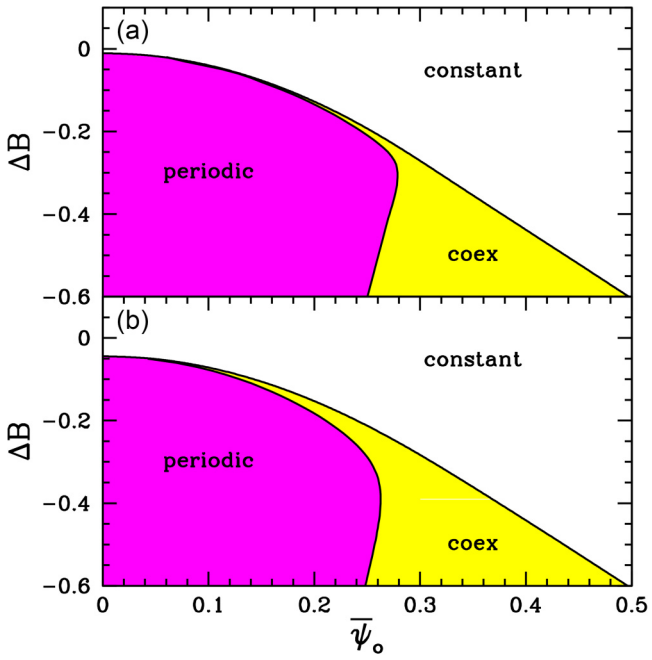

FIG. 2. Effective phase diagram for a strained one-dimensional system at (a) $\varepsilon = -0.0476$ and (b) $\varepsilon = -0.0909$.

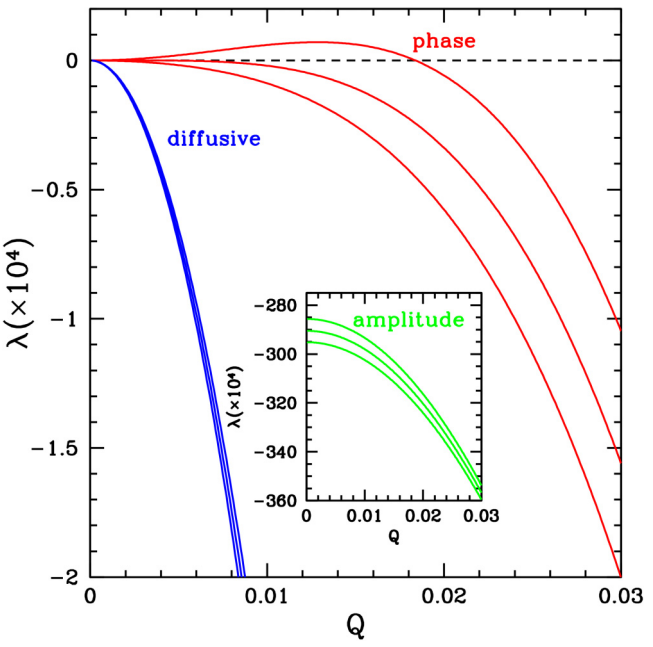

FIG. 3. Eigenvalue spectra for $(\Delta B, \bar{\psi}_o) = (-0.1374, 0.2)$. The red, blue, and green curves denote the three eigenvalues of the matrix $\mathbf{M}_Q$ defined in Eq. (11). For each color, the curves correspond (from bottom to top) to wave vectors $q = 1.029$, 1.030, and 1.031, respectively. The stability transition occurs at approximately $q_c \approx 1.030$, where the largest eigenvalue (top red curve) crosses zero (i.e., becomes positive), indicating the onset of exponential growth of perturbations at a finite wave number Q.

Before describing the full solution, it is instructive to consider a few limiting cases. More specifically, as discussed in Sec. III B, when the average mean density is fixed relatively simple expression for the critical value of ΔB can be obtained. The other simplifying case is when the average mean density is zero, which reveals three modes; a mass diffusion mode, a stable amplitude mode, and a phase mode that can become unstable as discussed in Sec. III C. Finally the general case is examined in Sec. III D.

B. Case 1: Constant mean density $\bar{\psi}_o$

We first consider the approximation $\psi_o = \bar{\psi}_0$, which suppresses mean density fluctuations. The linearized dynamics then reduce to

$$\frac{d}{dt}\begin{pmatrix}\delta\hat{A}\\ \delta\hat{A}^*\end{pmatrix} = \mathbf{M}_Q^{(2)}\begin{pmatrix}\delta\hat{A}\\ \delta\hat{A}^*\end{pmatrix}, \tag{16}$$

where

$$\mathbf{M}_Q^{(2)} = \begin{pmatrix}\hat{\mathcal{L}}_Q(\omega_{q+Q} - 2\omega_q) & -\hat{\mathcal{L}}_Q\,\omega_q\\ -\hat{\mathcal{L}}_{-Q}\,\omega_q & \hat{\mathcal{L}}_{-Q}(\omega_{q-Q} - 2\omega_q)\end{pmatrix}.$$

The instability threshold is determined by the condition that the largest eigenvalue $\lambda = 0$, i.e., $\det[\mathbf{M}_Q^{(2)} - \lambda\mathbf{I}] = 0$, where $\mathbf{I}$ is the identity matrix. Expanding this condition in the long-wavelength limit ($Q \to 0$) yields the critical quench depth

$$\begin{aligned}\Delta B_* &= -3\bar{\psi}_o^2 - (1-q^2)^2 - 4\frac{q^2(q^2-1)^2}{3q^2-1}\\ &\approx -3\bar{\psi}_o^2 - 12\varepsilon^2 + 28\varepsilon^3 - \mathcal{O}(\varepsilon^4) + \cdots.\end{aligned} \tag{17}$$

This describes a surface in the $(\epsilon, \bar{\psi}_o)$ plane, separating stable and unstable states, as shown in Fig. 4(a). The first term accounts for the crystal spinodal given by Eq. (8), while the other terms account for a strain-induced instability that can lead to a change in the crystalline periodicity. As expected, ΔB_* is not symmetric in ϵ as compressive strains are more energetically expensive than tensile strains.

C. Case 2: $\bar{\psi}_o = 0$ (mode decoupling)

In the limit $\bar{\psi}_o = 0$, the structure of the instability is most transparent. Here, $\beta = 0$ and the mean density perturbation $\delta\hat{\psi}_o$ decouples completely from the complex amplitude perturbations $\delta\hat{A}$ and $\delta\hat{A}^*$. As shown in Appendix C, the solutions can be written

$$\begin{bmatrix}\delta\hat{\psi}_o\\ \delta\hat{A}\\ \delta\hat{A}^*\end{bmatrix} = e^{-DQ^2t}\begin{bmatrix}1\\0\\0\end{bmatrix}c_o + e^{\lambda_+ t}\begin{bmatrix}0\\v_+\\1\end{bmatrix}c_+ + e^{\lambda_- t}\begin{bmatrix}0\\v_-\\1\end{bmatrix}c_-, \tag{18}$$

where $D = \Delta B + (1-Q^2)^2 - 2\omega_q$, and $v_\pm$, $\lambda_\pm$ are given in Appendix C. The constants c_0, $c_\pm$ are constants of integration, determined by boundary conditions. In the small-Q limit, $v_+ \to -1$ and $v_- \to +1$, which implies that the second term leads to changes in the imaginary part of δA while the third term modifies the real part, since $\delta A_I = (\delta A - \delta A^*)/(2i)$ and $\delta A_R = (\delta A + \delta A^*)/(2)$.

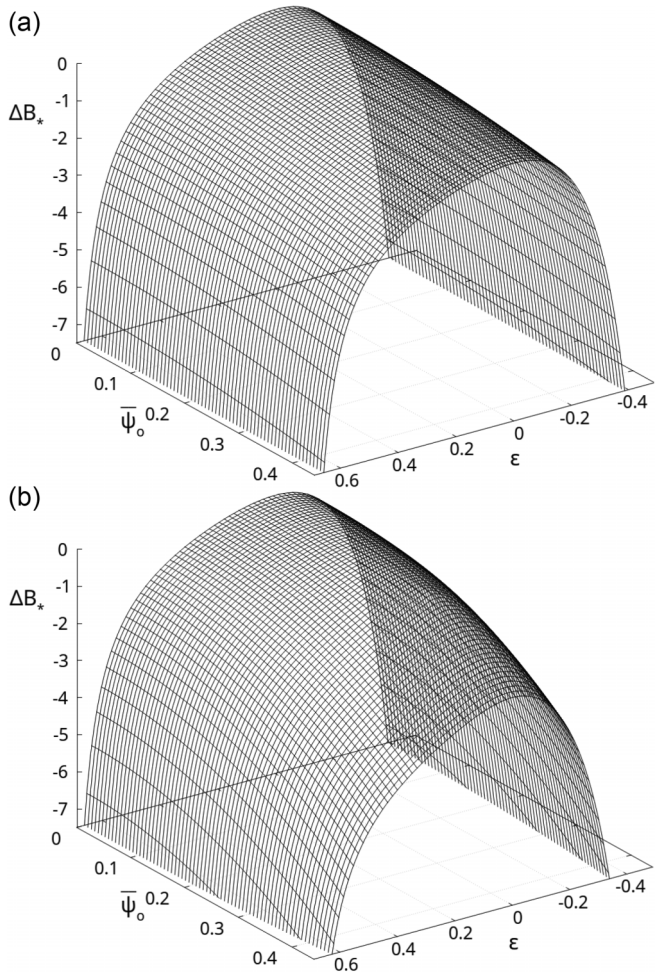

FIG. 4. Stability surface in the parameter space $(\bar{\psi}_o, \Delta B_*, \varepsilon)$, such that the system is stable (unstable) under (over) the surface. (a) corresponds to Eq. (17), which assumes ψ_o is constant and (b) corresponds to Eqs. (C10) and (C11), where ψ_o is allowed to vary.

This allows the identification of three distinct modes:

$$\delta\hat{\psi}_o \to e^{-D_0 Q^2 t}, \tag{19}$$

$$\delta\theta \to \mathrm{Im}(\delta\hat{A}) \to 2c_+ e^{\lambda_+ t}, \tag{20}$$

$$\delta|A| \to \mathrm{Re}(\delta\hat{A}) \to 2c_- e^{\lambda_- t}. \tag{21}$$

The first is a *diffusive mode* $\delta\hat{\psi}_o$: in the small-Q limit, $\delta\hat{\psi}$ decays exponentially at a rate $D_0 = D(Q \to 0) = \Delta B + 1 - 2\omega_q > 0$ in the solid state. To understand the other two modes, it is important to recognize that in the analysis the system was perturbed about a real solution [i.e., Eq. (7)]. Thus the real part of δA describes a change in amplitude of $|A|$, while the imaginary part can lead to changes in the phase (θ) of A. Thus, Eq. (20) describes a *phase mode* $\delta\theta$: since the only way for the phase to change (inducing a wavelength change) is for the imaginary part of δA to grow. This mode is responsible for phase slips and eventual changes in wave number. The third is a *magnitude mode* $\delta|A|$: this mode modulates the magnitude of the periodic state. Since the expansion is about a steady-state solution (i.e., a metastable minima), the amplitude mode is always stable.

Both $\delta\hat{\psi}_o$ and $\delta\theta$ are Goldstone modes characterized by $\lambda = 0$ at $Q = 0$, while the magnitude mode remains damped. The instability is therefore purely a *phase instability*, corresponding to long-wavelength distortions of the lattice and ultimately phase slips. The situation is much more complicated at larger values of $\bar{\psi}_o$, when melting can also occur, as discussed in the next section.

D. Case 3: $\bar{\psi}_o \neq 0$ (fully coupled system)

For finite $\bar{\psi}_o$, all modes are coupled. The instability threshold ΔB_* is obtained by expanding the largest eigenvalue at small Q and imposing $b_3 = 0$ [see Eq. (15)]. Solving this characteristic equation yields ω_q^* and ΔB_* as a function of $(\epsilon, \bar{\psi}_o)$, given by Eqs. (C9) and (C11), respectively, the main results of this work. ΔB_* describes a surface that separates linearly stable and unstable states and is shown in Fig. 4(b). A comparison of Figs. 4(a) and 4(b), indicates the approximation $\delta\psi_o = 0$ (which was employed in the original two-dimensional calculations of Goldenfeld *et al.* [23–26]) becomes increasing inaccurate as $\bar{\psi}_o$ increases, highlighting the importance of average density fluctuations in the stability of the periodic states. Other common approximations [8,26] in APFC modeling [such as setting $\mathcal{L} = -q^2$ in Eq. (5) or setting $(1 + \partial_{xx})^2 = 1$ in Eq. (6)] have no impact on the stability lines as those approximations have zero influence at $Q = 0$.

One important consequence of letting the density $\delta\psi$ vary is apparent even in the absence of strain. For $12\bar{\psi}_o^2 < 1$, a spinodal ΔB_s can be obtained at $\varepsilon = 1$, from Eq. (C12):

$$\Delta B_s = -3\bar{\psi}_o^2, \quad \bar{\psi}_o < 1/\sqrt{12}, \tag{22}$$

which reflects the second-order nature of the phase boundary above $\bar{\psi}_o = 1/\sqrt{12}$. However, below this point, in the coexistence region, the spinodal becomes [from Eq. (C12)]

$$\Delta B_s = 1 - 15\bar{\psi}_o^2, \quad \bar{\psi}_o > 1/\sqrt{12}, \tag{23}$$

which terminates at the coexistence line $\Delta B = -3\bar{\psi}_o^2$ at the critical point

$$\left(\bar{\psi}_o^c, \Delta B_c\right) = (\pm 1/\sqrt{12}, -1/4). \tag{24}$$

This different behavior is highlighted in Fig. 5, where the kink in the plot corresponds to entering the coexistence region.

For the more general case, it is instructive to consider the function $\omega_q^* = \Delta B_* + 3\bar{\psi}_o^2 + (1 - q^2)^2$, which, as discussed in Sec. II, incorporates the effective shift in the melting temperature due to global density $(3\bar{\psi}_o^2)$ and strain $(1 - q^2)$. Near $\epsilon = 0$ (or $q = 1$), this yields

$$\omega_q^* \approx \begin{cases} -\frac{8}{1-12\bar{\psi}_o}\epsilon^2 & \bar{\psi}_o < 1/\sqrt{12} \\ 1 - 12\psi_o^2 - 8\left[\frac{1-36\bar{\psi}_o^2}{1-12\bar{\psi}_o^2}\right]\epsilon^2 & \bar{\psi}_o > 1/\sqrt{12} \end{cases}. \tag{25}$$

These expressions reveal a qualitative change at $\bar{\psi}_o = 1/\sqrt{12}$, corresponding to the onset of liquid-solid coexistence, see Fig. 1.

For $\bar{\psi}_o = 0$, as discussed in Sec. III C, $\delta\hat{\psi}_o$ is completely decoupled from $\delta\hat{A}$ and $\delta\hat{A}^*$, and the instability is purely

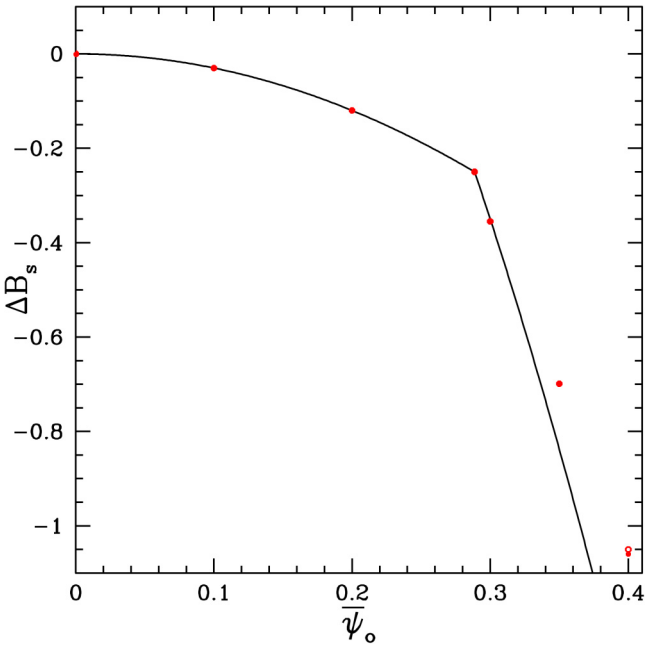

FIG. 5. Critical value of ΔB (ΔB_*) at $q = q_o$ versus $\bar{\psi}_o$. The lines correspond to analytic results and the points to numerical simulations of the full PFC model, i.e., Eq. (1).

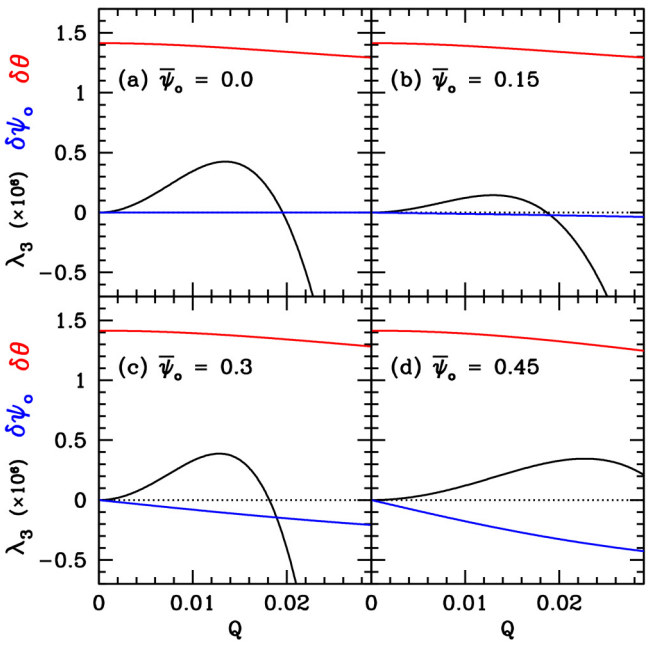

FIG. 6. Largest eigenvalue λ plotted in black as function of Q at $q = 1.031$ ($\epsilon = -0.03007$) at $\bar{\psi}_o = 0.0, 0.15, 0.3$, and 0.45 for (a), (b), (c), and (d), respectively. In addition the largest eigenvector, corresponding to $\delta\psi_o$, and the phase component $\delta\theta$ of δA are shown in blue and red respectively. The value of ΔB was chosen to be $\Delta B_*(\bar{\psi}_o, q = 1.03)$.

a phase mode. In this case, $\delta\hat{\psi}_o$ decays diffusively and the instability is completely induced by the strain for $q \neq 1$.

When $\bar{\psi}_o \neq 0$ the situation is more complicated. As $\bar{\psi}_o$ increases, the role of $\delta\psi_o$ plays an increasingly important role in the instability. As discussed in Appendix B, the (non-normalized) eigenvector for the most unstable mode can be obtained in the small-Q limit by assuming $\lambda = \alpha Q^2$, resulting in

$$\vec{v}_m = \begin{bmatrix} 1 \\ \eta_+/\chi \\ \eta_-/\chi \end{bmatrix}, \tag{26}$$

where expressions for $\eta_\pm$ and χ are given in Appendix B. In the small-Q limit, $\eta_+/\eta_- \to -1$, consistent with the phase-mode identification in the $\bar{\psi}_o = 0$ case. However, the first component of $\vec{v}_m$ (corresponding to $\delta\psi_o$) becomes significant for larger $\bar{\psi}_o$, indicating that the smoothed density itself participates in the instability. This thermodynamic instability typically becomes important in the liquid/solid coexistence regions, where it eventually leads to local melting of the lattice.

In Fig. 6 the largest eigenvalue and components of the corresponding important eigenvectors (i.e., the phase and diffusive modes) are shown for four different values of $\bar{\psi}_o$, with $q = 1.031$, where the value of ΔB was chosen to be $\Delta B_*(\bar{\psi}_o, q = 1.03)$. As can be seen in this figure, the eigenvector component corresponding to $\delta\psi_o$ is zero or very small for the two smaller values of $\bar{\psi}_o$ ($< \sqrt{1/12}$), but starts to play a role for larger values (i.e., $> \sqrt{1/12}$). For example, the magnitude of the density mode $\delta\psi$ is almost zero for small densities, but becomes more and more important as the average density increases, leading to instabilities in both the phase and density. This highlights the competition between mechanical and thermodynamic driving forces.

IV. NUMERICAL RESULTS

Direct numerical simulations of the full PFC model, i.e., Eq. (1), were conducted to study the stability of periodic states to small perturbations and compare with theoretical predictions. We consider an initial state

$$\psi = \bar{\psi}_o + 2A_s \cos(qx) + \eta(x), \tag{27}$$

where A_s is given by Eq. (7) and η was chosen to be a random number such that $-\delta < \eta(x) < \delta$ and $\langle\eta\rangle = 0$. Sample simulations for a small system ($L = 35a_o$) are presented in Fig. 7,

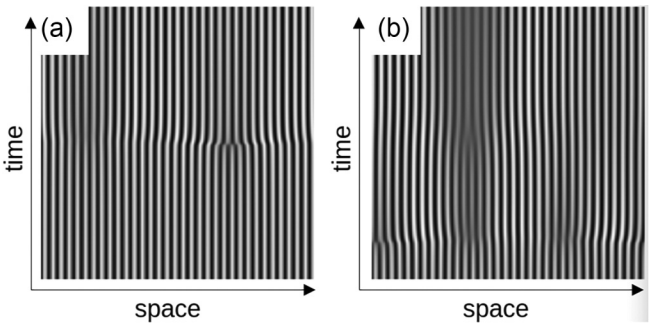

FIG. 7. Sample simulations at $(\Delta B, \epsilon) = (-0.4, -0.0476)$ illustrating the nature of the instability for (a) a simple phase slip at $\bar{\psi}_o = 0.3$ and (b) for a more complex process involving melting at $\bar{\psi}_o = 0.31$. The color scale ranges from $\psi = -0.25$ (black) to 0.8 (white) and the space range is from $x = 0$ to 209.45. The time scale corresponds to a region around the defect/melting events of size $\Delta t = 1100$.

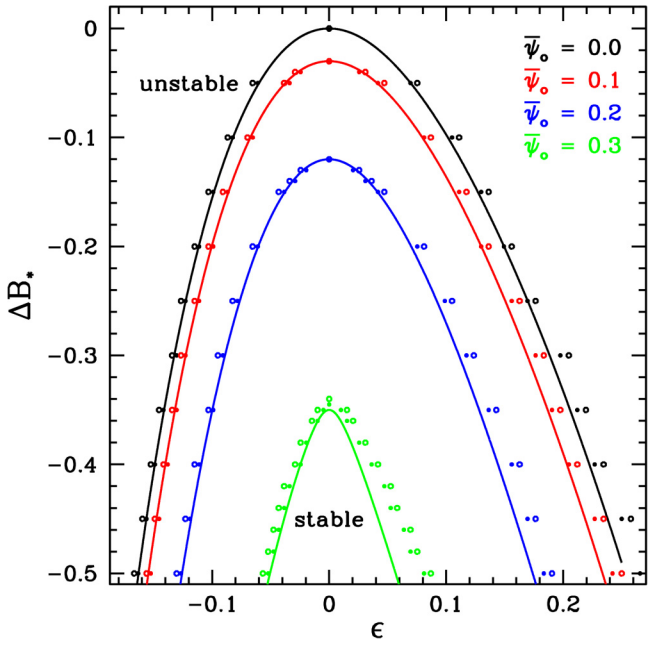

FIG. 8. Stability diagram: theory versus numerical simulations of the full PFC model, i.e., Eq. (1). In this figure the solid lines are from analytic calculations [i.e., Eqs. (C9) and (C11)]. The open (solid) symbols correspond to points at which the system was numerically unstable (stable) to small initial perturbations in ψ.

illustrating the result of the instability both when a single, simple phase slip occurs [see Fig. 7(a)] and when a more intricate process takes place, involving melting together with phase slips [see Fig. 7(b)]. Ideally, a linear stability analysis is only valid in the limit $\delta = 0$ and the system is infinite in size (since the initial instability occurs at $Q = 0$). Unfortunately, neither of these limits are numerically accessible. Despite these limitations δ was chosen as $\delta = 10^{-6}/2$ and the system size was $L = 200a_o$, where a_o is the equilibrium lattice constant, which was determined to be $a_o = 6.28356671$ numerically (differing slightly from the one-mode approximation $a_o = 2\pi/q_o = 2\pi$). A semispectral method (see Ref. [9], Appendix B 4) was used to evolve Eq. (1).

In a typical simulation, one of two possibilities arises: In one case the fluctuations die out and the total free energy only changes slightly. In the other, an instability occurs and there is a large change in the free energy. In some cases this jump corresponds to the start of a phase slip or change in wavelength, and in others to liquid/periodic phase separation (and also a potential change in wave number). Simulations were conducted for various values of ΔB and $\bar{\psi}_o$.

Because the system size is finite, only a discrete set of wave number q is allowed. More specifically, an integer N number of wavelengths must be used, such that the lattice constant would be L/N and corresponding wave number $q = 2\pi N/L$. Simulations were conducted to determine the value of N (and q and ϵ) just before and just after the linear stability. The results of the simulation are reported in Fig. 8 and show that the numerical simulations are in excellent quantitative agreement near $\epsilon = 0$ for all values of $\bar{\psi}_o$. For larger values of ϵ some deviations start to appear, likely due to assuming that the density can be represented by a single harmonic, an approximation that is valid at higher temperatures and lower strains.

V. DISCUSSION AND CONCLUSIONS

We have analyzed the linear stability of periodic states in the one-dimensional PFC model under applied strain and varying global mean density $\bar{\psi}_0$, using the amplitude formulation to simplify the analysis. Our main focus was to characterize the crossover between defect-mediated and spinodal-like instabilities, and to determine how strain ϵ, quench depth ΔB, and mean density $\bar{\phi}_o$ jointly control the onset of instability.

In the limit $\bar{\psi}_o = 0$, three decoupled modes were identified: a diffusive mode $\delta\psi_o$, a phase mode $\delta\theta$, and an amplitude mode $\delta|A|$. Both the diffusive and phase modes are Goldstone modes at $Q = 0$, while the amplitude mode is always gapped. The phase mode is solely responsible for the instability, which in this limit corresponds to a purely mechanical (elastic) phase slip.

For small $\bar{\psi}_0$ ($\bar{\psi}_0 < 1/\sqrt{12}$), the periodic state is stable at zero strain, and instability occurs only beyond a finite applied strain. In this regime, the unstable eigenmode lies primarily in the $(\delta A, \delta A^*)$ subspace, with negligible contribution from $\delta\psi_o$. Writing $A = |A|e^{i\theta}$, perturbations decompose as $\delta A = \delta|A| + i|A|\delta\theta$. Since magnitude fluctuations are gapped, while phase fluctuations correspond to the marginal $Q = 0$ mode associated with translational invariance, the softest direction is purely phaselike. The finite-Q instability therefore evolves from this marginal mode and is dominated by $\delta\phi$, corresponding to spatial variations of the displacement field, hence an elastic instability by phase slips.

For larger $\bar{\psi}_0$ ($\bar{\psi}_0 > 1/\sqrt{12}$), the system enters the coexistence region between periodic and uniform states, and the nature of the soft mode changes. As the liquid state becomes nearly degenerate, the cost of amplitude and density fluctuations is reduced, leading to a softening of $\delta|A|$ and its coupling to $\delta\psi_o$. The instability shifts toward coupled $(\delta|A|, \delta\psi_o)$ fluctuations, with a significant reduction of the amplitude magnitude and local density. This change in the soft mode redirects the instability from an elastic (phase-driven) mechanism to a spinodal-like instability, corresponding to local melting and the onset of liquid/solid coexistence. Numerical simulations of the full PFC dynamics from Eq. (1) confirm these predictions.

In summary, the amplitude formulation provides a transparent framework for linking linear stability to the underlying physical mechanisms of melting. The marginal $Q = 0$ mode reflects global phase invariance, while finite-Q instabilities select between phase-dominated (elastic) and density-dominated (spinodal) modes depending on the mean density $\bar{\psi}_0$. This density-dependent shift of the soft mode unifies defect-mediated and spinodal melting in one dimension, and provides insight into higher-dimensional systems, where these mechanisms correspond to dislocation nucleation, vacancy formation, and partial melting in strained crystalline solids or colloidal systems. It will also be interesting to see how other factors such as impurities or complex lattices with sublattice ordering will impact the stability of solid phases.

ACKNOWLEDGMENTS

K.R.E. and B.A. acknowledge support of the National Science Foundation (NSF) under Grant No. DMR-2006456 and Oakland University Technology Services and high-performance research computing facility (Matilda).

DATA AVAILABILITY

There are no publicly available research data or software supporting this manuscript. Requests for further information or data should be sent to the authors.

APPENDIX A: RESCALING

The basic phase-field-crystal model in one dimension can be written in field (n) related to the atomic number density [20] as

$$\mathcal{F}' = \int dx' \left[\frac{\Delta B'}{2} n^2 + \frac{B'_x}{2} n \left(q_o^2 + \partial_{x'x'}\right)^2 n - \frac{t}{3} n^3 + \frac{v}{4} n^4 \right], \tag{A1}$$

where $\Delta B'$ controls the liquid/solid (constant/periodic) transition and as such acts like a temperature, B'_x determines the magnitude of the elastic moduli, and q_o determines the length scale of the pattern. The dynamics are assumed dissipative and conserved, i.e.,

$$\frac{\partial n}{\partial t'} = \tau \partial_{x'x'} \frac{\delta \mathcal{F}'}{\delta n}, \tag{A2}$$

where, τ controls the time scales. More details on these parameters can be found in Elder *et al.* [20]. While this model contains a number of parameters it is convenient to make several variable changes to reduce this number.

Making the following variable changes in Eqs. (1) and (2),

$$x = x' q_o, \tag{A3}$$

$$\psi = (n - t/3v)\left(v/q_o^4 B_x\right)^{1/2}, \tag{A4}$$

$$\Delta B = (\Delta B' - t^2/3v)/\left(q_o^4 B'_x\right), \tag{A5}$$

$$\mathcal{F} = \mathcal{F}' v/\left(q o^7 B_x^2\right), \tag{A6}$$

$$t = v^{1/2}/\left(\tau q_o^8\right) t', \tag{A7}$$

gives

$$\mathcal{F} = \int dx \left[\frac{\Delta B}{2} \psi^2 + \frac{\psi}{2} (1 + \partial_{xx})^2 \psi + \frac{\psi^4}{4} \right] \tag{A8}$$

and

$$\frac{\partial \psi}{\partial t} = \nabla_x^2 \frac{\delta \mathcal{F}}{\delta \psi} = \nabla_x^2 [(\Delta B + (1 + \nabla_{xx})^2)\psi + \psi^3], \tag{A9}$$

where terms in the free energy that do not impact the dynamics (i.e., constant or linear in ψ) have been dropped.

APPENDIX B: EVOLUTION MATRIX

The linearized equations of the perturbation fields are given by

$$\begin{aligned}
\frac{\partial \delta\psi_o}{\partial t} &= \partial_{xx}\left[\left(\Delta B + 3\psi_o^2 + 6A_s^2 + (1 + \partial_{xx})^2\right)\delta\psi_o + 6A_s\bar{\psi}_o(\delta A + \delta A^*)\right], \\
\frac{\partial \delta A}{\partial t} &= \mathcal{L}\left[\left(\Delta B + 3\psi_o^2 + 6A_s^2 + (1 + \mathcal{L})^2\right)\delta A + 3A_s^2\delta A^* + 6A_s\bar{\psi}_o\delta\psi\right], \\
\frac{\partial \delta A^*}{\partial t} &= \mathcal{L}\left[\left(\Delta B + 3\psi_o^2 + 6A_s^2 + (1 + \mathcal{L})^2\right)\delta A^* + 3A_s^2\delta A + 6A_s\bar{\psi}_o\delta\psi\right],
\end{aligned}$$

using that A_s is real valued. In the Fourier space, the evolution equations for perturbed fields around a steady-state crystal state are

$$\begin{aligned}
\frac{\partial \delta\hat{\psi}_0}{\partial t} &= -Q^2\left[\left(\Delta B + 3\psi_o^2 - 2\omega_q + (1 - Q^2)^2\right)\delta\hat{\psi}_o + \beta(\delta\hat{A} + \delta\hat{A}^*)\right], \\
\frac{\partial \delta\hat{A}}{\partial t} &= \hat{\mathcal{L}}_Q\left[\left(\Delta B + 3\psi_o^2 - 2\omega_q + (1 - (Q + q)^2)^2\right)\delta\hat{A} - \omega_q\delta\hat{A}^* + \beta\delta\hat{\psi}_o\right], \\
\frac{\partial \delta\hat{A}^*}{\partial t} &= \hat{\mathcal{L}}_{-Q}\left[\left(\Delta B + 3\psi_o^2 - 2\omega_q + (1 - (Q - q)^2)^2\right)\delta\hat{A}^* - \omega_q\delta\hat{A} + \beta\delta\hat{\psi}_o\right],
\end{aligned}$$

using that $\hat{\mathcal{L}}_{\pm Q} = -Q^2 \mp 2qQ - q^2 = -(Q \pm q)^2$. We can write this in vector form

$$\frac{\partial \vec{y}}{\partial t} = \mathbf{M}_Q \vec{y}, \tag{B1}$$

where the evolution matrix $\mathbf{M}$ is given in Eq. (11), using the notation

$$\begin{aligned}
\omega_Q &= \Delta\tilde{B} + (1 - Q^2)^2, \\
\omega_{q\pm Q} &= \Delta\tilde{B} + (1 - (Q \pm q)^2)^2.
\end{aligned}$$

The eigenvector for the most unstable mode can be obtained in the small-Q limit by assuming $\lambda = \alpha Q^2$, giving (for $\bar{\psi}_o \neq 0$)

$$\vec{v}_m = \begin{bmatrix} 1 \\ \eta_+/\chi \\ \eta_-/\chi \end{bmatrix}, \tag{B2}$$

where

$$\eta_\pm = -2\bar{\psi}_o\sqrt{-3\omega_q}(Q \mp q)^2[Q^5 \mp 2Q^4 q - (2+q^2)Q^3 \pm 4Q^2 q^3 + (\alpha - 2q^4 + 6q^6)Q \pm 4q^3(1-q^2)] \tag{B3}$$

and

$$\begin{aligned}\chi = Q[&Q^{10} - 2(3q^2+2)Q^8 + (13q^4 + 16q^2 + 2\alpha - 2\omega_q + 4)Q^6 + (-28q^6 + 12q^4 - 2(4\omega_q + \alpha + 12)q^2 \\ &+ 4(\omega_q - \alpha))Q^4 + (36q^8 - 56q^6 + 2(11\omega_q - 2\alpha + 18)q^4 + 4(3\alpha - 2\omega_q)q^2 - 2\alpha\omega_q + \alpha^2)Q^2 - 16q^{10} \\ &+ 32q^8 - 4(3\omega_q + 4)q^6 + 4q^4\omega_q - 2\alpha q^2\omega_q].\end{aligned} \tag{B4}$$

Equations (B3) and (B4) indicate a divergence in the ratio $\eta_\pm/\chi$. However, the initial conditions are such that $\delta\psi(Q=0, t=0) = \delta A(Q=0, t=0) = 0$, so that this divergence is eliminated. It is interesting to note that in the small-Q limit, the ratio η_+/η_- goes to -1:

$$\frac{\eta_+}{\eta_-} = -1 + \frac{6q^4 - 2q^2 + \alpha}{2q^5 - 2q^3}Q + \mathcal{O}(Q^2) + \cdots, \tag{B5}$$

similar to the $\bar{\psi}_o = 0$ case.

APPENDIX C: CRITICAL ΔB

The critical value of ΔB at which a periodic solution becomes unstable will be denoted ΔB^*. The value of ΔB^* can be obtained by solving for the eigenvalues of the matrix $\mathbf{M}$ given in Eq. (11). In general, this gives rise to a cubic equation and lengthy expressions for the eigenvalues, which greatly simplify in the limit $\bar{\psi}_o = 0$.

1. Limit: $\bar{\psi}_o = 0$

In this case, $\beta = 0$, so that the matrix $\mathbf{M}$ reduces such that the smoothed density $\delta\psi$ is completely decoupled from the complex amplitude δA. The solutions can be written

$$\begin{aligned}\delta\hat{\psi} &= e^{-Q^2(\Delta B + (1-Q^2)^2)t}c_o, \\ \begin{bmatrix} \delta\hat{A} \\ \delta\hat{A}^* \end{bmatrix} &= e^{\lambda_+ t}\begin{bmatrix} v_+ \\ 1 \end{bmatrix}c_+ + e^{\lambda_- t}\begin{bmatrix} v_- \\ 1 \end{bmatrix}c_-,\end{aligned} \tag{C1}$$

where c_o and $c_\pm$ are determined by boundary conditions and the eigenvalues $\lambda_\pm$ and eigenvectors $v_\pm$ are given as

$$\lambda_\pm = 2Q^2q^4 + (Q^4 - 6Q^2 + \omega_q)q^2 - Q^6 + 2Q^4 + Q^2\omega_q \pm \sqrt{4q^2Q^2\beta(\beta + 2\omega_q) + (Q^2+q^2)\omega_q^2}, \tag{C2}$$

$$\lambda_+ \approx \left[\frac{2(4q^8 - 8q^6 + q^4(4 + 3\omega_q) - \omega_q q^2)}{\omega_q}\right]Q^2 + \mathcal{O}(Q^4)\cdots, \tag{C3}$$

$$\lambda_- \approx 2q^2\omega_q - \left[\frac{2(4q^8 - 8q^6 + q^4(4 + 3\omega_q) - \omega_q q^2)}{\omega_q}\right]Q^2 + \mathcal{O}(Q^4)\cdots, \tag{C4}$$

$$v_\pm = \frac{(Q-q)^2\omega_q}{2qQ(\alpha + \omega_q) \pm \sqrt{4q^2Q^2\beta(\beta + 2\omega_q) + (Q^2+q^2)\omega_q^2}} \approx \mp 1 + \mathcal{O}(Q) + \cdots. \tag{C5}$$

Solving for the value of ω_q (ω_q^*) when the sign of the coefficient of Q^2 in Eq. (C3) changes gives

$$\omega_q^* = -\frac{4q^2(1-q^2)^2}{3q^2 - 1}, \tag{C6}$$

or in terms of the critical $\Delta B_* = \omega_q^* - (1-q^2)^2$,

$$\Delta B_* = -\frac{7q^2 - 1}{3q^2 - 1}(1-q^2)^2. \tag{C7}$$

It should also be noted that a similar solution arises if it is assumed that the smoothed density ψ_o is constant, i.e., $\psi_o = \bar{\psi}_o$. In this instance it is straightforward to show that

$$\begin{aligned}\Delta B_* &= -3\bar{\psi}_o^2 - \frac{7q^2-1}{3q^2-1}(1-q^2)^2 \\ &\approx -3\bar{\psi}_o^2 - 12\varepsilon^2 + 28\varepsilon^3 - 63\varepsilon^4 + \cdots .\end{aligned} \tag{C8}$$

The $-3\psi_o^2$ follows the line of second-order phase transitions shown in Fig. 1 for $\bar{\psi}_o^2 < 1/12$. Thus, if the smoothed density is not allowed to vary the quantity $[\Delta B_* + 3\psi_o^2]$ is independent of $\bar{\psi}_o$ if $\delta\psi_o = 0$.

2. Limit: $\bar{\psi}_o \neq 0$

In this limit, $\delta\psi_o$ does not decouple from the complex amplitude and the solutions for the eigenvalues and vectors are more complex. However, since the instability first occurs at $Q = 0$, it is possible to find more tractable solutions to the cubic eigenvalue equation by setting $\lambda \approx -\alpha Q^2$, substituting into the eigenvalue equation, and solving to order Q^4. Solving for the value of ΔB_* (when $\alpha = 0$) gives ω_q^* (where $\Delta B_* = \omega_q^* - 3\bar{\psi}_o^2 - (1-q^2)^2$):

$$\begin{aligned}\omega_q^* = &\frac{q^2(-7q^4+15q^2-6) + 12\bar{\psi}_o^2(1-3q^2)}{6q^2-2} \\ &- \frac{\sqrt{144(3q^2-1)^2\bar{\psi}_0^4 + 24q^2(21q^6-52q^4+33q^2-6)\bar{\psi}_0^2 + q^4(q^4-q^2+2)^2}}{6q^2-2}\end{aligned} \tag{C9}$$

$$\approx \begin{cases} -\frac{2}{1-12\bar{\psi}_o^2}(1-q^2)^2 + \cdots & = -\frac{8}{1-12\bar{\psi}_o^2}\epsilon^2 + \cdots & \bar{\psi}_o^2 < 1/12 \\ -2(1-q^2)^2 + (1-q^2)^3 + \cdots & = -8\epsilon^2 + 16\epsilon^3 + \cdot & \bar{\psi}_o^2 = 1/12 \\ 1 - 12\bar{\psi}_o^2 - \frac{1-36\bar{\psi}_o^2}{1-12\bar{\psi}_o^2}(1-q^2)^2 + \cdots & = 1 - 12\bar{\psi}_o^2 - 4\frac{1-36\bar{\psi}_o^2}{1-12\bar{\psi}_o^2}\epsilon^2 + \cdots & \bar{\psi}_o^2 > 1/12 \end{cases}, \tag{C10}$$

where the $\pm$ sign in Eq. (C10) corresponds to $q < 1$ (+) and $q > 1$ (−). The result can easily be translated to the critical ΔB_*:

$$\Delta B_* = \omega_q^* - 3\bar{\psi}_o^2 - (1-q^2)^2 \tag{C11}$$

$$\approx \begin{cases} -3\bar{\psi}_o^2 - 12\frac{1-4\bar{\psi}_o^2}{1-12\bar{\psi}_o^2}\epsilon^2 + 4\frac{7-36\bar{\psi}_o^2}{1-12\bar{\psi}_o^2}\epsilon^3 - \mathcal{O}\epsilon^4 \cdots & \bar{\psi}_o^2 < 1/12 \\ 1 - 15\bar{\psi}_o^2 - 8\frac{24\bar{\psi}_o^2-1}{12\bar{\psi}_o^2-1}\epsilon^2 + 24\frac{20\bar{\psi}_o^2-1}{12\bar{\psi}_o^2-1}\epsilon^3 - \mathcal{O}\epsilon^4 \cdots & \bar{\psi}_o^2 > 1/12 \end{cases}. \tag{C12}$$

[1] J. M. Kosterlitz and D. J. Thouless, Metastability and phase transitions in two-dimensional systems, J. Phys. C **6**, 1181 (1973).

[2] J. M. Kosterlitz, The critical properties of the two-dimensional xy model, J. Phys. C **7**, 1046 (1974).

[3] W. W. Gerberich, J. C. Nelson, E. T. Lilleodden, P. Anderson, and J. T. Wyrobek, Indentation induced dislocation nucleation: The initial yield point, Acta Mater. **44**, 3585 (1996).

[4] C. L. Kelchner, S. J. Plimpton, and J. C. Hamilton, Dislocation nucleation and defect structure during surface indentation, Phys. Rev. B **58**, 11085 (1998).

[5] A. E. Mayer, V. S. Krasnikov, and V. V. Pogorelko, Homogeneous nucleation of dislocations in copper: Theory and approximate description based on molecular dynamics and artificial neural networksa, Comput. Mater. Sci. **206**, 111266 (2022).

[6] S. Kumari and A. Dutta, Nucleation of twinning dislocation loops in fcc metals, Mech. Mater. **160**, 103934 (2021).

[7] S. Aubry, K. Kang, S. Ryu, and W. Cai, Energy barrier for homogeneous dislocation nucleation: Comparing atomistic and continuum models, Scr. Mater. **64**, 1043 (2011).

[8] M. Salvalaglio and K. R. Elder, Coarse-grained modeling of crystals by the amplitude expansion of the phase-field crystal model an overview, Modelling Simul. Mater. Sci. Eng. **30**, 053001 (2022).

[9] N. Provatas and K. Elder, *Phase-Field Methods in Materials Science and Engineering* (John Wiley & Sons, Weinheim, Germany, 2011).

[10] V. Skogvoll, A. Skaugen, L. Angheluta, and J. Viñals, Dislocation nucleation in the phase-field crystal model, Phys. Rev. B **103**, 014107 (2021).

[11] Y. Yang, Z. Yan, H. Liu, J. Shen, and W. Kang, Spinodal decomposition as a possible void initialization mechanism for spallation in shock melted materials under high strain rates, Phys. Rev. E **111**, 035406 (2025).

[12] F. Vidal, T. W. Johnston, J.-C. Kieffer, and F. Martin, Spallation induced by ultrashort laser puleses at critical tension, Phys. Rev. B **70**, 184125 (2004).

[13] V. I. Levitas, B. F. Henson, L. B. Smilowitz, and B. W. Asay, Solid-solid phase transformation via virtual melting significantly below the melting temperature, Phys. Rev. Lett. **92**, 235702 (2004).

[14] V. I. Levitas, Crystal-amorphous and crystal-crystal phase transformations via virtual melting, Phys. Rev. Lett. **95**, 075701 (2005).

[15] Q. An, S.-N. Luo, L.-B. Han, L. Zheng, and O. Tschauner, Melting of Cu under hydrostatic and shock wave loading to high pressures, J. Phys.: Condens. Matter **20**, 095220 (2008).

[16] V. I. Levitas and R. Ravelo, Virtucal melting as new mechanism of stress relaxation under high strain rate loading, Proc. Natl. Acad. Sci. USA **109**, 13204 (2012).

[17] H. Chen and V. I. Levitas, Virtual melting and cyclic transformations between amorphous Si, Si I, and Si IV in a shear band at room temperature, npj Comput. Mater. **11**, 59 (2025).

[18] K. R. Elder, M. Katakowski, M. Haataja, and M. Grant, Modeling elasticity in crystal growth, Phys. Rev. Lett. **88**, 245701 (2002).

[19] K. R. Elder and M. Grant, Modeling elastic and plastic deformations in nonequilibrium processing using phase field crystals, Phys. Rev. E **70**, 051605 (2004).

[20] K. R. Elder, N. Provatas, J. Berry, P. Stefanovic, and M. Grant, Phase-field crystal modeling and classical density functional theory of freezing, Phys. Rev. B **75**, 064107 (2007).

[21] M. Salvalaglio, L. Angheluta, Z.-F. Huang, A. Voigt, K. R. Elder, and J. Vinals, A coarse-grained phase-field model of plastic motion, J. Mech. Phys. Solids **137**, 103856 (2020).

[22] V. Skogvoll, L. Angheluta, A. Skaugen, M. Salvalaglio, and J. Vinals, A phase field crystal theory of kinematics of dislocation lines, J. Mech. Phys. Solids **166**, 104932 (2022).

[23] B. P. Athreya, G. Nigel, and J. A. Dantzig, Renormalization-group theory for the phase field crystal model, Phys. Rev. E **74**, 011601 (2006).

[24] N. Goldenfeld, B. P. Athreya, and J. A. Dantzig, Renormalization group approach to multiscale simulation of polycrystalline materials using the phase field crystal model, Phys. Rev. E **72**, 020601(R) (2005).

[25] B. P. Athreya, N. Goldenfeld, J. A. Dantzig, M. Greenwood, and N. Provatas, Adaptive mesh computation of polycrystalline pattern formation using a renormalization-group reduction of the phase-field crystal model, Phys. Rev. E **76**, 056706 (2007).

[26] D.-H. Yeon, Z.-F. Huang, K. Elder, and K. Thornton, Density-amplitude formulation of the phase-field crystal model for two-phase coexistence in two and three dimensions, Philos. Mag. **90**, 237 (2010).